ELSEVIER

Powder Technology 85 (1995) 1–9

POWDER TECHNOLOGY

A hypoplastic constitutive model for cohesive powders

E. Bauer [a], W. Wu [b]

[a] *Institute of Mechanics, Graz University of Technology, Graz, Austria*
[b] *Lahmeyer International Ltd, Frankfurt am Main, Germany*

Received 6 May 1994; revised 15 January 1995

Abstract

A simple extension of an incrementally nonlinear, so-called hypoplastic constitutive model, which was originally proposed for cohesionless sand, is presented with respect to cohesive powders. Motivated by the effect of capillary force, an internal state variable representing an intrinsic pressure is introduced. The model is then extended by adding the intrinsic pressure to the actual stress. The material parameters in the extended model can be identified with conventional experiments. Numerical simulations of several laboratory tests, including oedometer and triaxial tests, are presented. By comparing the predicted relation between tensile strength and consolidation pressure with experimental data on limestone powder available in the literature, it is shown that the extended model is capable of reproducing the salient behaviour of cohesive powders, e.g. the nonlinear stress–strain relation, dilatant volume change upon shearing and the dependence of the tensile strength on the consolidation pressure.

Keywords: Cohesive powders; Intrinsic pressure; Stress; Tensile strength; Shearing

1. Introduction

Bulk solids can be classified grossly into cohesive and cohesionless materials according to how the resistance against shearing is developed. Whereas the shear resistance of cohesionless materials, such as sand, is of frictional nature, the shear resistance of cohesive materials may be caused by different chemical and physical effects, for example van der Waals and capillary bounds or cementation. A substantial difference between cohesive and cohesionless materials on the macroscopic level lies in the fact that cohesive materials are able to sustain tensile stress up to a certain limit while cohesionless materials cannot.

The description of the mechanical behaviour of bulk solids is important in a number of engineering fields, such as geotechnical or chemical engineering and the handling in silos. In the latter area, cohesive materials often result in unwelcome phenomena such as choking and arching. Traditionally, the results from model tests often serve as the basis for engineering design and constructive dimensioning [1,2]. However, the model tests suffer from the shortcoming that the results cannot be related to problems with different boundary conditions and loading histories.

Recently, much effort has been devoted to the research of constitutive models for bulk solids [3,4]. A perusal of the relevant literature suggests, however, that most constitutive models proposed for bulk solids are based on elastoplastic theory. Although remarkable success has been reported in the literature [5], there seem to be some potential difficulties in applying elastoplastic models. Upon deviatoric loading bulk solids generally do not show a clear yielding point and an elastic domain cannot be identified. Furthermore, the deformation during unloading is not totally reversible. As a consequence, the determination of the yield surface and the decomposition of the deformation into elastic and plastic parts are rather questionable. A general overview of the basic differences between the various constitutive models, i.e. hyperelasticity, hypoelasticity, hyperplasticity or elastoplasticity and hypoplasticity can be found in the recent work by Wu and Niemunis [6].

The paper focuses on cohesive materials with limestone powder as the representative material and presents the so-called hypoplastic model as an alternative approach to the elastoplastic constitutive models. The hypoplastic model is based on nonlinear tensorial functions and is developed without recourse to the concepts in elastoplastic theory such as yield surface, flow rule and the decomposition of the deformation into elastic and plastic parts. The idea of using nonlinear tensorial functions to describe the mechanical behaviour of cohesionless sand was pioneered by Kolymbas [7]. By adopting a specific function, it was shown that many salient features of sand could be reproduced. In a later work

SSDI 0032-5910(95)02999-I

by Wu and Kolymbas [8], the definition of hypoplasticity was given and the general form of the hypoplastic constitutive model was proposed. Based on this general constitutive model, various aspects of cohesionless materials have been investigated, such as shear banding [9], cyclic loading [10], rate dependence [11] and failure [12]. The hypoplastic model has been shown to capture the salient features of granular materials. Remarkable progress has been achieved in the recent work by Wu and Bauer [13] where the critical state was integrated successfully into the hypoplastic model to account for the effect of the stress level and the initial density on the mechanical behaviour of sand. The proposed constitutive model covers a broad spectrum of density and is applicable to both initial and fully developed plastic deformations.

Motivated by the formal similarity between the behaviour of loose sand and normally consolidated cohesive powders and between dense sand and overconsolidated cohesive powders, the present investigation continues and enlarges the line of work by Wu and Bauer [13] to account for cohesion and the effect of strain history.

In Section 2 the framework of the hypoplastic constitutive model is briefly recapitulated. In Section 3, the constitutive model is extended by introducing an internal state variable, which depends on the stress level and the void ratio. The identification of the material parameters in the model is discussed in Section 4. Finally, the capability of the constitutive model is demonstrated by simulating laboratory tests on limestone powders in Section 5.

2. Outline of the hypoplastic model

We start with the general constitutive equation of the rate type and assume that the Jaumann stress rate $\mathring{\boldsymbol{T}}$ depends on the Cauchy stress $\boldsymbol{T}$ and the stretching $\boldsymbol{D}$:

$$\mathring{\boldsymbol{T}} = \boldsymbol{H}(\boldsymbol{T}, \boldsymbol{D}) \tag{1}$$

The Jaumann stress rate is defined by

$$\mathring{\boldsymbol{T}} = \dot{\boldsymbol{T}} - \boldsymbol{W}\boldsymbol{T} + \boldsymbol{T}\boldsymbol{W} \tag{2}$$

where the spin tensor $\boldsymbol{W}$ and the stretching tensor $\boldsymbol{D}$ are related to the velocity $\boldsymbol{v}$ as follows:

$$\boldsymbol{D} = \tfrac{1}{2}[\nabla \boldsymbol{v} + (\nabla \boldsymbol{v})^{\mathrm{T}}],\quad \boldsymbol{W} = \tfrac{1}{2}[\nabla \boldsymbol{v} - (\nabla \boldsymbol{v})^{\mathrm{T}}] \tag{3}$$

In accordance with the notations of continuum mechanics [14] italic bold lower and upper case letters are used to denote vectors and tensors. A superposed dot implies material time differentiation. Following the sign convention in continuum mechanics tensile stress, elongative strain and their rates are taken as positive. The principle of material objectivity requires that the constitutive equation must be frame indifferent. For a detailed formulation of Eq. (1) the general representation theorem for an isotropic tensor-valued function of two symmetric tensors given by Wang [15] can be used:

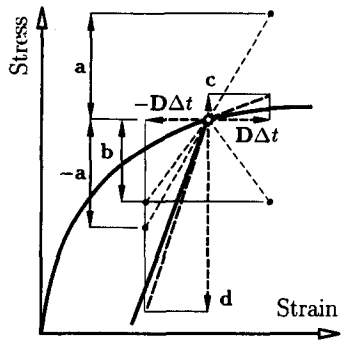

Fig. 1. Strain and stress response of the hypoplastic model.

$$\begin{aligned}\mathring{\boldsymbol{T}} = {} & \alpha_1 \boldsymbol{I} + \alpha_2 \boldsymbol{T} + \alpha_3 \boldsymbol{D} + \alpha_4 \boldsymbol{T}^2 + \alpha_5 \boldsymbol{D}^2 + \alpha_6 (\boldsymbol{T}\boldsymbol{D} + \boldsymbol{D}\boldsymbol{T}) \\ & + \alpha_7 (\boldsymbol{T}\boldsymbol{D}^2 + \boldsymbol{D}^2\boldsymbol{T}) + \alpha_8 (\boldsymbol{T}^2\boldsymbol{D} + \boldsymbol{D}\boldsymbol{T}^2) \\ & + \alpha_9 (\boldsymbol{T}^2\boldsymbol{D}^2 + \boldsymbol{D}^2\boldsymbol{T}^2)\end{aligned} \tag{4}$$

where α_i $(i = 1, \ldots, 9)$ are scalar functions of the invariants and joint invariants of the tensors $\boldsymbol{T}$ and $\boldsymbol{D}$:

$$\begin{aligned}\alpha_i = \alpha_i (& \mathrm{tr}(\boldsymbol{T}), \mathrm{tr}(\boldsymbol{T}^2), \mathrm{tr}(\boldsymbol{T}^3), \mathrm{tr}(\boldsymbol{D}), \mathrm{tr}(\boldsymbol{D}^2), \mathrm{tr}(\boldsymbol{D}^3), \\ & \mathrm{tr}(\boldsymbol{T}\boldsymbol{D}), \mathrm{tr}(\boldsymbol{T}^2\boldsymbol{D}), \mathrm{tr}(\boldsymbol{T}\boldsymbol{D}^2), \mathrm{tr}(\boldsymbol{T}^2\boldsymbol{D}^2))\end{aligned} \tag{5}$$

The advantage of Eq. (4) lies in the fact that terms with a higher order than two can be expressed by their irreducible integrity bases. The construction of coefficients α_i by the invariants allows an infinite multiplicity. However, the number of material constants should not be too high to allow for an easy calibration of the constitutive model.

It was shown by Wu and Kolymbas [8] that the following tensorial function is suitable for capturing the incremental nonlinear behaviour of granular materials:

$$\mathring{\boldsymbol{T}} = \boldsymbol{L}(\boldsymbol{T}, \boldsymbol{D}) + \boldsymbol{N}(\boldsymbol{T})\,\|\boldsymbol{D}\| \tag{6}$$

where $\|\cdot\|$ denotes the Euclidean norm. Eq. (6) consists of two parts, namely a linear tensorial function $\boldsymbol{L}(\boldsymbol{T}, \boldsymbol{D})$ in $\boldsymbol{D}$ and a nonlinear function $\boldsymbol{N}(\boldsymbol{T})\,\|\boldsymbol{D}\|$ in $\boldsymbol{D}$.

It should be noted that the concepts in elastoplasticity theory, such as yield surface, plastic potential and decomposition into elastic and plastic parts, are not used in developing Eq. (6). There is even no need to define loading and unloading explicitly, since they are specified implicitly by the equation. To show how loading and unloading can be accounted for, let us consider two cases, namely two stretchings with the same length $\|\boldsymbol{D}\|$ but in opposite directions, $\boldsymbol{D}$ and $-\boldsymbol{D}$. The principle of our hypoplastic model in describing loading and unloading is depicted in Fig. 1. The response of Eq. (6) can be separated into the response of the linear part and of the nonlinear part. For the stretchings $\boldsymbol{D}$ and $-\boldsymbol{D}$, we obtain two stress rates with the same length and in opposite directions from the linear part ($\dot{\boldsymbol{a}}$ and $-\dot{\boldsymbol{a}}$ in Fig. 1). The nonlinear part, however, yields the same stress rate ($\dot{\boldsymbol{b}}$ in Fig. 1) irrespective of the direction of stretching. The response of the equation, which is composed of the sum of the contributions from the linear and the nonlinear parts, is $\dot{\boldsymbol{c}}$ for loading $\boldsymbol{D}$ and $\dot{\boldsymbol{d}}$ for unloading $-\boldsymbol{D}$. In this way, the irreversible behaviour during

loading and unloading can be accounted for with a single constitutive equation. It is worth noting that the nonlinear part is active for both loading and unloading.

From the positive homogeneity of first degree if $\boldsymbol{D}$ follows the rate independence of the hypoplastic model. The nonlinearity in $\boldsymbol{D}$ implies the possibility of describing dissipative material behaviour as well. An explicit form of Eq. (6) was proposed by Wu [16]:

$$\mathring{\boldsymbol{T}} = C_1 \operatorname{tr}(\boldsymbol{T})\boldsymbol{D} + C_2 \frac{\operatorname{tr}(\boldsymbol{TD})}{\operatorname{tr}(\boldsymbol{T})}\boldsymbol{T} + C_3 \frac{\boldsymbol{T}^2}{\operatorname{tr}(\boldsymbol{T})}[\operatorname{tr}(\boldsymbol{D}^2)]^{1/2} + C_4 \frac{\boldsymbol{T}_{\mathrm{dev}}^2}{\operatorname{tr}(\boldsymbol{T})}[\operatorname{tr}(\boldsymbol{D}^2)]^{1/2} \quad (7)$$

wherein the deviatoric stress $\boldsymbol{T}_{\mathrm{dev}}$ is given by

$$\boldsymbol{T}_{\mathrm{dev}} = \boldsymbol{T} - \tfrac{1}{3}\operatorname{tr}(\boldsymbol{T})\boldsymbol{I}$$

with $\boldsymbol{I}$ as the unit tensor. The determination of the dimensionless constants C_i and the simulation of laboratory tests have been described [16,17].

It should be noted that the limit state of a granular material is also included in the hypoplastic constitutive equation. A material element is said to be in a limit state if the stiffness vanishes for particular $\boldsymbol{T}$ and $\boldsymbol{D}$ satisfying $\mathring{\boldsymbol{T}} = \boldsymbol{0}$. For Eq. (6), the limit state leads to a conical surface with its apex in the origin of the principal stress space [12].

3. The extended hypoplastic model

In Eq. (6), the history dependence is assumed to be represented by the instantaneous stress alone. While this assumption has been shown to be reasonable for simple loading programmes, e.g. monotonic loading, it is certainly oversimplified for more complex loading programmes. Moreover, Eq. (7) is homogeneous in stress. In the principal stress space, the limit surface is a cone with its apex at the origin. Therefore, equations such as Eq. (1) allow no tensile stress. The above shortcomings can be removed by extending the constitutive equation with an internal state variable $\boldsymbol{S}$:

$$\mathring{\boldsymbol{T}} = \boldsymbol{H}(\boldsymbol{T}, \boldsymbol{S}, \boldsymbol{D}) \quad (8)$$

$\boldsymbol{S}$ is assumed to be a symmetric tensor of second order. The objective rate $\mathring{\boldsymbol{S}}$ is assumed to be determined by the following general form:

$$\mathring{\boldsymbol{S}} = \boldsymbol{M}(\boldsymbol{T}, \boldsymbol{S}, \boldsymbol{D}) \quad (9)$$

The dependence of $\boldsymbol{S}$ on the loading history may be obtained by integration of Eq. (9). It is worth noting that different chemical or physical causes for cohesion give rise to a different material behaviour. In the present paper the evolution equation for $\boldsymbol{S}$ is focused on granular materials like limestone powder where cohesion is assumed to depend on the average distance between the grains. The effects of cementation and the change of water content are not taken into account. From experiments we know that cohesion

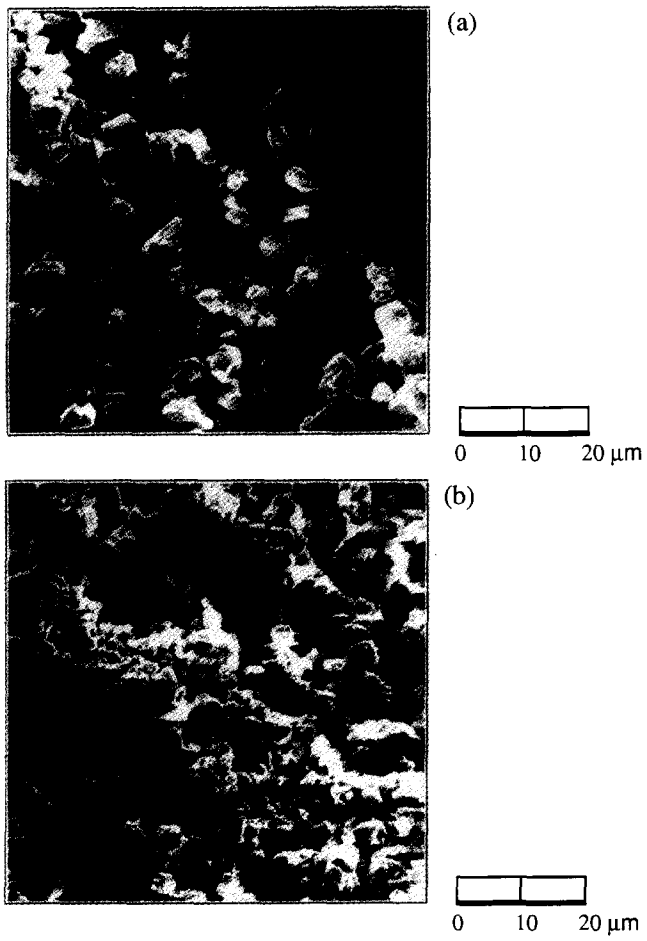

Fig. 2. Limestone powder (a) before and (b) after consolidation.

depends primarily on the strain history. An initially loose powder will become denser with increasing consolidation pressure. After full unloading the swelling is smaller and the memory on the overconsolidation stress is evident by a lower void ratio. During reloading the compressive strength increases with the overconsolidation stress. The microscope picture in Fig. 2 shows the variation of the distance between the limestone particles before and after the consolidation. Inspired by the experimental results that for a given stress level the shear resistance depends on the compaction of the material, the evolution equation for $\mathring{\boldsymbol{S}}$ is assumed to be a function of the volumetric strain rate $\operatorname{tr}(\boldsymbol{D})$ and $\boldsymbol{S}$ itself:

$$\mathring{\boldsymbol{S}} = -k_1 \boldsymbol{S} \operatorname{tr}(\boldsymbol{D}) \quad (10)$$

where k_1 is a positive material parameter.

Motivated by the kinematic hardening concept of Ziegler [18] the following stress transformation can be used:

$$\boldsymbol{T}^* = \boldsymbol{T} + \boldsymbol{S} \quad (11)$$

We incorporate the internal state variable $\boldsymbol{S}$ in Eq. (6) by replacing the stress tensor $\boldsymbol{T}$ with a transformed stress tensor $\boldsymbol{T}^*$:

$$\mathring{\boldsymbol{T}} = \boldsymbol{L}(\boldsymbol{T}^*, \boldsymbol{D}) + \boldsymbol{N}(\boldsymbol{T}^*)\|\boldsymbol{D}\| \quad (12)$$

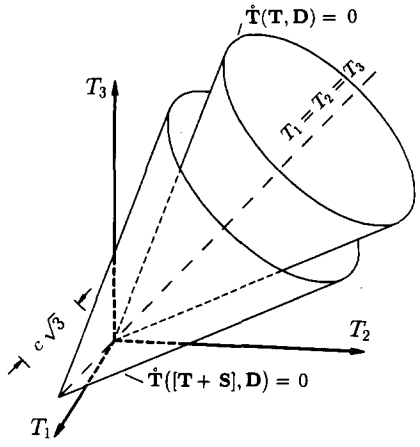

Fig. 3. Limit surfaces in the principal stress space.

The meaning of the transformed stress can be illustrated by comparison of Eqs. (6) and (12) in the limit state (Fig. 3). Considering an isotropic internal state variable $\boldsymbol{S} = c\boldsymbol{I}$, the meaning of the stress transformation $\boldsymbol{T} + \boldsymbol{S}$ can be shown by shifting the apex of the limit surface along the space diagonal $T_1 = T_2 = T_3$ back with a distance of $c\sqrt{3}$ from the origin.

If the internal state variable $\boldsymbol{S}$ changes with the deformation process, which is evident for the present case using Eq. (10), the limit surface depends on the strain history. Starting from an initial $\boldsymbol{S}_0$ the absolute value of $\boldsymbol{S}$ will increase during contraction, where $\mathring{\boldsymbol{S}}$ is proportional to $\boldsymbol{S}$ and the volumetric strain rate. For dilatation the value of $\boldsymbol{S}$ decreases and approaches zero asymptotically. If the compressibility of the grains is negligibly small, the strain rate in Eq. (10) can be expressed by the void ratio e and its rate $\dot{e}$:

$$\mathring{\boldsymbol{S}} = -k_1 \boldsymbol{S} \frac{\dot{e}}{1+e} \tag{13}$$

It should be noted that the influence of an inherent anisotropic cohesion can be described by the same hypoplastic constitutive model with an anisotropic initial tensor $\boldsymbol{S}_0$. The eigendirection of $\boldsymbol{S}$ is independent of volume change and the memory of the initial direction will not be swept out. Stress-induced anisotropic phenomena are not included in Eq. (13). To take into account the dependence of $\mathring{\boldsymbol{S}}$ on $\boldsymbol{T}$ an extension of Eq. (10) is conceivable. However, it is obvious that a refined reproduction of the material behaviour usually requires a larger number of material constants and experimental data for the calibration. The experimental investigation of the anisotropic behaviour is rather extensive and does not belong to the standard laboratory tests. For simplicity we neglect anisotropic effects and consider in the following an initial isotropic tensor $\boldsymbol{S}_0$. With respect to a void ratio $e = e_0$ and an intrinsic isotropic stress c_0:

$$\boldsymbol{S}_0 = c_0 \boldsymbol{I} \tag{14}$$

the components S_i ($i = 1, 2, 3$) in Eq. (13) can be evaluated by analytical integration:

$$S_i = c(1+e)^{-k_1} \tag{15}$$

The value of c in Eq. (15) carries the dimension of stress and can be estimated either by the parameters c_0, e_0, k_1:

$$c = c_0(1+e_0)^{k_1} \tag{16}$$

or as the internal state variable for a vanishing void ratio $e = 0$. A detailed calibration will be outlined in Section 4. Eqs. (15) and (16) show that for the special constitutive assumptions of Eqs. (13) and (14), the value of $\boldsymbol{S}$ can be represented by the current void ratio. It is worth noting that other causes of cohesion need different representations of the evolution equation for $\boldsymbol{S}$, e.g. the change of the water content and the effect of cementation cannot be related to the void ratio alone.

To incorporate strain softening as a material behaviour depending on the density and the stress level, we get the following extended constitutive equation:

$$\mathring{\boldsymbol{T}} = I_s[\boldsymbol{L}(\boldsymbol{T}^*, \boldsymbol{D}) + I_e \boldsymbol{N}(\boldsymbol{T}^*) \|\boldsymbol{D}\|] \tag{17}$$

with

$$\boldsymbol{L}(\boldsymbol{T}^*, \boldsymbol{D}) = C_1 \operatorname{tr}(\boldsymbol{T}+\boldsymbol{S})\boldsymbol{D} + C_2 \frac{\operatorname{tr}((\boldsymbol{T}+\boldsymbol{S})\boldsymbol{D})}{\operatorname{tr}(\boldsymbol{T}+\boldsymbol{S})}(\boldsymbol{T}+\boldsymbol{S})$$

$$\boldsymbol{N}(\boldsymbol{T}^*) = C_3 \frac{(\boldsymbol{T}+\boldsymbol{S})^2}{\operatorname{tr}(\boldsymbol{T}+\boldsymbol{S})} + C_4 \frac{(\boldsymbol{T}+\boldsymbol{S})_{\mathrm{dev}}^2}{\operatorname{tr}(\boldsymbol{T}+\boldsymbol{S})}$$

The stiffness factor I_s and density factor I_e stand for the effect of pyknotropy and barotropy.

There is experimental evidence that the stress response of a material for the same stress state and the same deformation direction is also influenced by the current void ratio. The deformation resistance of a material will increase with increasing density. If we neglect the anisotropic effect, the behaviour can be described only by scalar multiplication of the basic hypoplastic equation with a stiffness factor I_s as a function of the void ratio. The stiffness factor I_s in Eq. (17) is assumed to be

$$I_s = \left(\frac{e_{i0}}{e}\right)^{p_1} \tag{18}$$

Herein $p_1 > 1$ and the reference void ratio e_{i0} are constants. A decrease of the void ratio e means an increase of the stiffness factor I_s and consequently an increase in the stress rate, i.e. for the same stress state and stretching the stress rate derived from Eq. (17) is higher for a lower void ratio.

An increase in the peak friction angle with the density can be taken into account by a scalar multiplication of the nonlinear part of the constitutive equation with I_e. The density factor I_e in Eq. (17) is defined by

$$I_e = \left(\frac{e - e_d}{e_c - e_d}\right)^{p_2} \tag{19}$$

where e is the current void ratio, e_c the critical void ratio, e_d the maximum void ratio and p_2 a constitutive constant. The

void ratio e changes during the deformation according to the following equation:

$$\dot{e} = (1+e)\ \mathrm{tr}(\boldsymbol{D}) \tag{20}$$

Comparison of the current void ratio with the critical void ratio allows differentiating between normal consolidation and overconsolidation:

normal consolidation $e > e_c$
overconsolidation $e < e_c$

Within the density factor in Eq. (19) the concept of the critical state [19] is included in the extended hypoplasticity model. A critical state is defined by stationary stress and a stationary void ratio under continuing shear deformation, namely as a limit state with $\mathring{\boldsymbol{T}} = \boldsymbol{0}$ and $\dot{e} = 0$. For stationary flow there is no change of volume and hence $\mathring{\boldsymbol{S}} = \boldsymbol{0}$. For $e = e_c$ we obtain $I_e = 1$ and consequently Eq. (17) in the limit state is related to the critical one. This fact will be taken into account by the calibration of the constitutive constants C_i ($i = 1, ..., 4$) as outlined in Section 4. The friction angle in a critical state will be denoted as φ_c. A lower void ratio $e < e_c$ leads to $I_e < 1$, which means that the influence of the nonlinear part of the constitutive equation decreases and for $\mathring{\boldsymbol{T}} = \boldsymbol{0}$ a higher peak friction angle $\varphi > \varphi_c$ will be obtained.

For the maximum void ratio $e = e_d$ the value of the density factor I_e is zero and the stress rate is only a function of the linear part of Eq. (17):

$$\mathring{\boldsymbol{T}} = I_s\, \boldsymbol{L}(\boldsymbol{T}^*, \boldsymbol{D})$$

In this case the constitutive equation becomes hypoelastic according to the definition given by Truesdell [14]. This means, for instance, that cyclic loading starting from $e = e_d$ does not result in further densification.

There is experimental evidence that the critical void ratio decreases with an increasing stress level. The dependence of e_c on the transformed stress level $\boldsymbol{T}^*$ can be described by

$$e_c = e_{c0} \exp\{-[\mathrm{tr}(\boldsymbol{T}^*/p_0)]^{p_3}\} \tag{21}$$

where e_{c0} is the critical void ratio for the reference pressure p_0. It is assumed that the lower bound of the void ratio, e_d decreases with $\mathrm{tr}(\boldsymbol{T}^*)$ in a similar manner as e_c:

$$e_d = e_{d0} \exp\{-[\mathrm{tr}(\boldsymbol{T}^*/p_0)]^{p_3}\} \tag{22}$$

4. Identification of material parameters

The extended hypoplastic model, Eq. (17) includes 12 parameters: the four parameters C_1, C_2, C_3, C_4 of the basic version, k_1, c for the internal state in Eq. (15), p_1, e_{i0} and e_{d0} for the dependence of the stiffness on the current void ratio and the three constants p_2, p_3, e_{c0} for the influence of pyknotropy and barotropy on limit states, i.e. on peak strengths and stationary flow states.

The following calibration procedure is based on experimental data of triaxial tests with different consolidation stresses. For a homogeneous deformation the direction of the principal strain and stress rates are coaxial and the Jaumann stress rate $\mathring{\boldsymbol{T}}$ is equal to the material time derivation $\dot{\boldsymbol{T}}$. In the coordinate system (T_1, T_2, T_3), due to axial symmetry of the triaxial test, we have $D_2 = D_3$ and $T_2 = T_3$. For this boundary condition Eq. (17) leads to two independent differential equations:

$$\dot{T}_1 = C_1(T_1^* + 2T_3^*)D_1 + C_2 \frac{T_1^* D_1 + 2T_3^* D_3}{T_1^* + 2T_3^*} T_1^* + \left[C_3 T_1^{*2} + \frac{4}{9} C_4 (T_1^* - T_3^*)^2\right] \frac{(D_1^2 + 2D_3^2)^{1/2}}{T_1^* + 2T_3^*} \tag{23}$$

$$\dot{T}_3 = C_1(T_1^* + 2T_3^*)D_3 + C_2 \frac{T_1^* D_1 + 2T_3^* D_3}{T_1^* + 2T_3^*} T_3^* + \left[C_3 T_3^{*2} + \frac{1}{9} C_4 (T_1^* - T_3^*)^2\right] \frac{(D_1^2 + 2D_3^2)^{1/2}}{T_1^* + 2T_3^*} \tag{24}$$

with

$$T_i^* = T_i + S_1,\ i = 1, 3 \tag{25}$$

For triaxial compression the axial strain rate is assumed to be $D_1 = -1$. It should be noted that the absolute value of D_1 is immaterial, as the constitutive equation is rate independent.

First we consider a stationary flow state (T_{1c}, T_{3c}, e_c) defined by $\mathring{\boldsymbol{T}} = \boldsymbol{0}$ and $\mathrm{tr}(\boldsymbol{D}) = 0$. The density factor in this state is $I_e = 1$ and the value of the stiffness factor I_s has no influence on the constitutive equation. It is worth noting that the stress ratio T_{1c}/T_{3c} for stationary flow is influenced by S_1 and not constant in contrast to a cohesionless granular material. From Eqs. (23) and (24) we obtain the following relation:

$$\frac{T_{1c} + S_{1c}}{T_{3c} + S_{1c}} = \text{constant} \tag{26}$$

With respect to Eq. (15) the internal variable in Eq. (26) can be expressed by the void ratio $e = e_c$:

$$\frac{T_{1c} + c(1+e_c)^{-k_1}}{T_{3c} + c(1+e_c)^{-k_1}} = \text{constant} \tag{27}$$

Inserting the values for T_{1c}, T_{3c} and the corresponding void ratio e_c from triaxial compression tests with different consolidation pressures in Eq. (27), we obtain a set of equations for the approximation of the parameters c and k_1.

The decrease of the void ratio with the consolidation pressure referring to a stationary flow state can be described by Eq. (21) where the parameters e_{c0} and p_3 can be fitted to the data of critical states, i.e. to the relation between e_c and $\mathrm{tr}(\boldsymbol{T}^*) = T_{1c} + 2T_{3c} + 3c(1+e_c)^{-k_1}$. It is assumed in Eq. (22) that the changing of the lowest void ratio e_d with $\boldsymbol{T}^*$ is affine to the critical void ratio e_c. The value e_{d0} is defined as the maximum density of the granular structure under $\boldsymbol{T}^* = \boldsymbol{0}$

and can be approximated by a simple shaking test with small amplitudes.

The calibration of the four constants C_1, C_2, C_3, C_4 can be carried out using the following quantities from the triaxial compression test with an initial void ratio $e = e_{10}$:

(i) in the isotropic consolidation state:

the tangential stiffness $\dot{T}_1/D_1 = E_0$

with respect to $I_s = 1$ and $S_{01} = c(1+e_{10})^{-k_1}$

the stress state $T_1 = T_3 = T_0$

the ratio of the strain rates $\dfrac{D_3}{D_1} = \nu_0$

(ii) and in the stationary flow state:

the stress ratio $\dfrac{T_{1c}+S_{1c}}{T_{3c}+S_{1c}} = a_c$

with respect to $S_{1c} = c(1+e_c)^{-k_1}$

the ratio of the strain rates $\dfrac{D_3}{D_1} = 0.5$

The constitutive equation yields the following four linear equations in a matrix form:

$$\begin{bmatrix} 3 & \frac{1}{3}(1-2\nu_0) & -\frac{(1+2\nu_0^2)^{1/2}}{3} & 0 \\ 9\nu_0 & 2\nu_0-1 & (1+2\nu_0^2)^{1/2} & 0 \\ -(a_c+2)^2 & a_c(1-a_c) & \sqrt{\frac{3}{2}}\,a_c^2 & \frac{4}{9}\sqrt{\frac{3}{2}}\,(a_c-1)^2 \\ \frac{1}{2}(a_c+2)^2 & 1-a_c & \sqrt{\frac{3}{2}} & \frac{1}{9}\sqrt{\frac{3}{2}}\,(a_c-1)^2 \end{bmatrix} \times \begin{Bmatrix} C_1 \\ C_2 \\ C_3 \\ C_4 \end{Bmatrix} = \begin{Bmatrix} \frac{E_0}{T_0+S_{01}} \\ 0 \\ 0 \\ 0 \end{Bmatrix}$$

The solution to this equation system leads to the parameters C_i $(i = 1, 2, 3, 4)$.

The tangential stiffness at the beginning of a triaxial compression is proportional to the pressure level and refers to E_0 and the void ratio in accordance with the data used for the calibration. From experimental evidence, it can be seen that different stiffnesses for the same initial triaxial compression level are caused by different densities depending on the deformation history. For higher consolidation pressures e will decrease and the initial tangential stiffness will increase. The influence of the void ratio is included in the extended model by the stiffness factor $(e_{10}/e)^{p_i}$. The value e_{10} refers to the triaxial test for the calibration of the constants C_i. The different tangential stiffnesses for various overconsolidation ratios can be approximated by the following relation:

$$\dot{T}_1/D_1 = E_0\left(\frac{e_{10}}{e}\right)^{p_i} \tag{28}$$

Following the triaxial compression test the stiffness will decrease with increasing axial load and approaches zero if the shear resistance is fully mobilized. The peak strength is higher for a denser material under lower pressure. Strain softening can be observed after the peak and the void ratio will increase asymptotically to the critical value. For a strain-controlled test the shear resistance after the peak will decrease while the void ratio increases asymptotically to the critical value. The limit state for a normally consolidated material is reached for large axial deformation while a peak cannot be observed. It should be noted that the limit state at the peak defined by $\dot{\boldsymbol{T}} = \boldsymbol{0}$ does not fulfil the condition of $\mathrm{tr}(\boldsymbol{D}) = 0$ for the critical state. For cohesionless granular materials Wu and Bauer [13] showed that the influence of barotropy and pyknotropy on the peak strength and strain softening can be described by a density factor I_e. A similar adaptation of the density factor defined in Eq. (19) can be found for cohesive powders. With the known relation for e_c and e_d the parameter p_2 can be optimized by numerical simulations of the peak strength for different overconsolidated states. The numerical experiments show that the parameter p_2 lies in a small range between $0.02 < p_2 < 0.25$.

It should be noted that the homogeneity of the specimen is usually limited for large deformations by strain localizations. Therefore the assumption of stationary flow is only pragmatic for numerical reasons, e.g. to limit the dilatancy for large shearing. A further remark should be made concerning localized deformations in the form of shear bands at large straining. Shear band formation is often accompanied by pronounced strain softening. As soon as shear bands appear, the experimental results cannot be evaluated. Nevertheless, there is experimental evidence that moderate strain softening can still be observed without shear bands. After shear bands occur, the stress–strain behaviour generally depends on the thickness of the shear bands. One possible way to describe this behaviour is to extend the constitutive model to include a so-called internal length [20]. Since our model does not possess an internal length, its application is limited to the regime prior to shear band formation.

5. Numerical simulations

The performance of the model will be illustrated by simulating normally consolidated and overconsolidated triaxial tests with different consolidation stresses. The determination of material parameters is based on the experimental data from triaxial tests with limestone powder. With the calibration procedure described in the above section the set of parameter

Table 1
Constants for the numerical experiments

C_1	C_2	C_3	C_4
−12.34	−108.12	−109.27	107.77
e_{i0}	e_{c0}	e_{d0}	k_1
1.1	2.45	0.4	22.9
c (kPa)	p_1	p_2	p_3
−0.0001	2.05	0.18	0.049

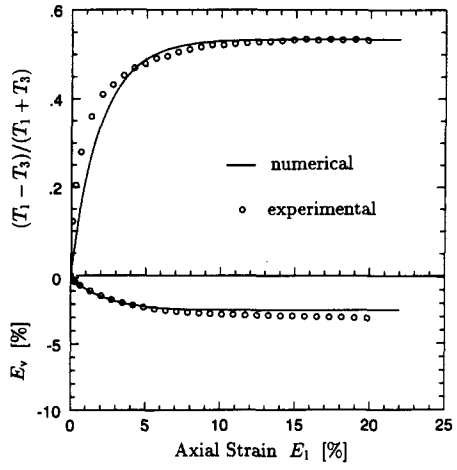

Fig. 4. Numerical and experimental triaxial compression test. Experimental data from limestone powder with a consolidation stress $T_0 = 95$ kPa [10].

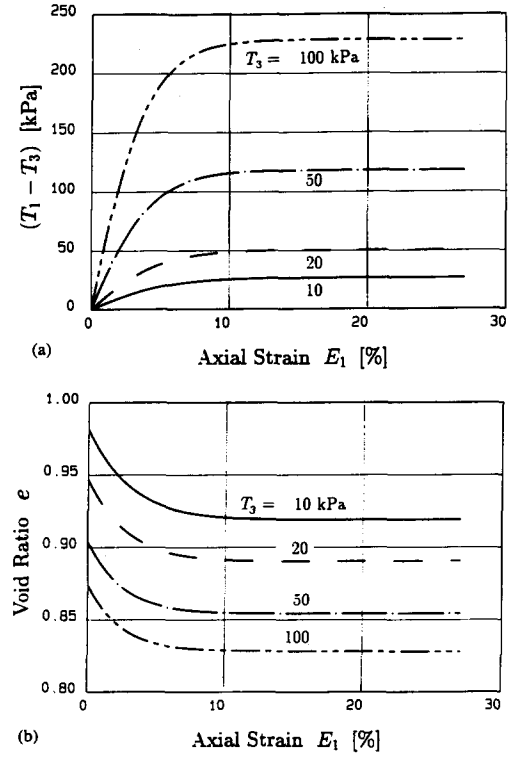

Fig. 5. Triaxial compression test with different normal consolidation pressure.

values given in Table 1 is obtained where the reference pressure in Eqs. (21) and (22) is $p_0 = 100$ kPa. It should be noted that the preparation of tests on powders is very difficult. Some hints about sample preparation are given by Harder [21] and Bauer [17]. The critical state with vanishing volume change was not reached in experiments. Therefore the present calibration is rather qualitative in order to show the essential features of the proposed constitutive model.

Fig. 4 shows the numerical prediction of a triaxial compression test together with the experimental data for a consolidation pressure of $T_0 = 95$ kPa. A numerical investigation of consolidation pressure on the material behaviour is given in Fig. 5. For normally consolidated triaxial compression tests the strain and stress paths reach a stationary value asymptotically and the void ratio in the critical state is lower for a higher consolidation pressure. The influence of cohesion can be shown in uniaxial compressive tests (Fig. 6) and uniaxial tensile tests (Fig. 7) with $T_2 = T_3 = 0$. The initial void ratios are dependent on isotropic compression and extension. A relation between the initial density and the maximum compressive or the tensile strengths is evident. For the same consolidation pressure the compressive strength is higher than the maximum tensile stress. The strength increases with overconsolidation pressure and shows softening after the peak with dilatation. With respect to the relation between the internal variable $\boldsymbol{S}$ and the void ratio, Eq. (15), dilatation also means a reduction of $\boldsymbol{S}$. A relation between the compressive strength and the consolidation stress is shown in Fig. 8 together with experimental results from Schwedes and

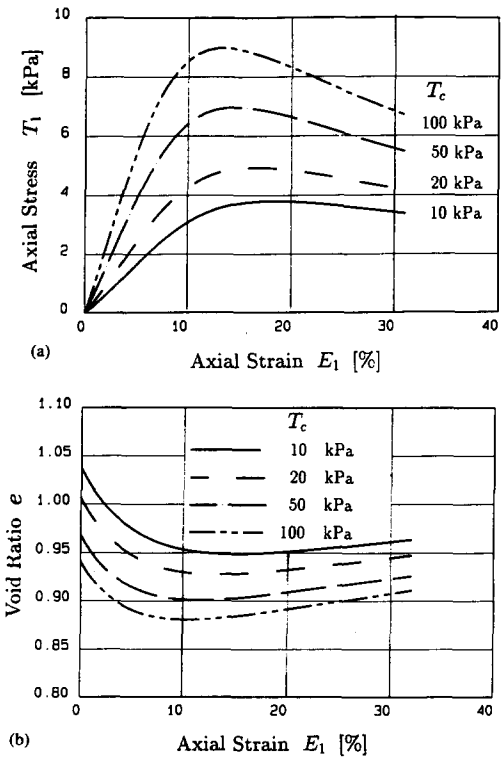

Fig. 6. Uniaxial compressive strength for different consolidation pressures.

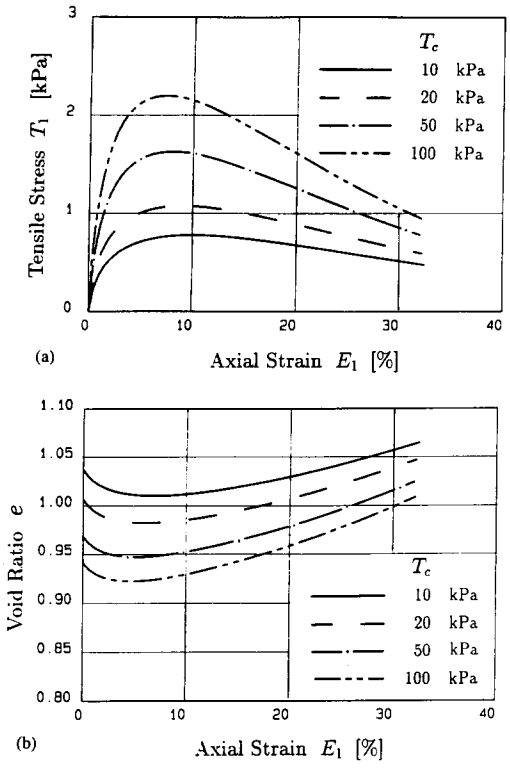

Fig. 7. Tensile test for different consolidation pressures.

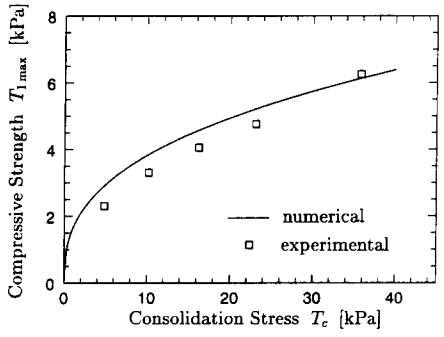

Fig. 8. Compression strength versus consolidation stress.

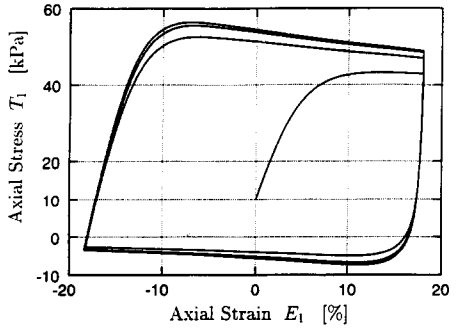

Fig. 9. Numerical triaxial test under cyclic loading with a confining pressure of 10 kPa and an initial consolidation pressure of 100 kPa.

Schulze [22]. The numerical simulation shows that the nonlinear relation is more significant for low consolidation stress levels and goes over to a linear relation for higher consolidation pressure.

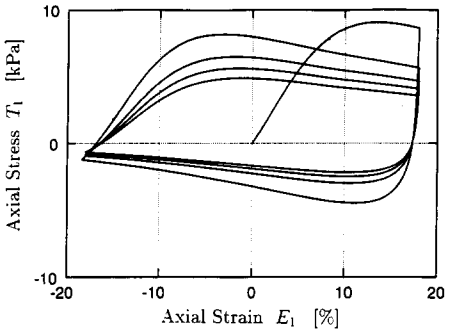

Fig. 10. Numerical experiment of an uniaxial cyclic loading test with an initial consolidation pressure of 100 kPa.

Finally, we will investigate the influence of overconsolidation during cyclic loading tests with a symmetric strain amplitude of $E_1 = \pm 18\%$. Firstly we will consider a cyclic triaxial test under a constant confining pressure of 10 kPa after a virgin isotropic compression to 100 kPa. As shown in Fig. 9 the magnitude of the deviatoric stress is higher for compression than for extension. With an increasing cycle number the maximum deviatoric stress increases. After several cycles a shake-down will be reached. Fig. 10 shows the result of a similar cyclic test which was isotropically consolidated to 100 kPa and then completely unloaded. The maximum axial stress decreases with the number of cycles and gradually approaches a limit value. Comparison of Fig. 10 with Fig. 9 shows that the influence of the overconsolidation ratio on the stress–strain behaviour is significant.

6. Conclusions

Our objective was to present a hypoplastic model for granular materials with cohesion. The basic hypoplastic model was extended by introducing an internal state variable and a density factor. Consequently, it has been shown that stiffness, contractancy and dilatancy are dependent on density and the stress level; that cohesion depends on the deformation history expressed by the void ratio; and that strain softening after the peak until a residual friction resistance is possible.

7. List of symbols

a_c	stress ratio in critical state
c_0	internal state variable with dimension of stress for $e = e_0$
C_i	$(i = 1, 2, 3, 4)$ constitutive constants
$\boldsymbol{D}$	stretching tensor
D_i	$(i = 1, 2, 3)$ principal strain rates
e	void ratio
$\dot{e}$	rate of e

e_c void ratio in a critical state
e_d minimum void ratio
E_0 initial tangential stiffness in triaxial compression corresponding to void ratio e_{i0}
E_i $(i=1, 2, 3)$ principal strain
$\boldsymbol{I}$ identity tensor
I_e density factor
I_s stiffness factor
k_1 dimensionless constitutive constant
p_0 reference pressure
p_i $(i=1, 2, 3)$ constitutive constants for pyknotropy and barotropy
$\mathring{\boldsymbol{S}}$ objective rate of internal state variable $\boldsymbol{S}$
S_i $(i=1, 2, 3)$ components of internal state variable $\boldsymbol{S}$
$\boldsymbol{T}$ Cauchy stress tensor
$\dot{\boldsymbol{T}}$ time derivation of Cauchy stress tensor
$\mathring{\boldsymbol{T}}$ Jaumann stress rate
$\dot{T}_i$ $(i=1, 2, 3)$ principal stress rates
T_0 isotropic consolidation stress
T_i $(i=1, 2, 3)$ principal stresses
$\boldsymbol{W}$ spin tensor

Greek letter

ν_0 Poisson ratio for $e=e_{i0}$

Acknowledgements

The paper is a partial result of a research project supported by the German Research Community (SFB 219 Silo) under the supervision of Professor G. Gudehus and Professor D. Kolymbas.

References

[1] J. Williams, *Powder Technol., 1* (1967) 189.
[2] J. Williams, *Powder Technol., 4* (1970/71) 328.
[3] W.A.M. Brekelmans, *Powder Technol., 62* (1990) 21.
[4] D. Bortzmeyer, *Powder Technol., 70* (1992) 131.
[5] H.W. Höhl and J. Schwedes, *Powder Technol., 70* (1992) 31.
[6] W. Wu and A. Niemunis, *Proc. Third Int. Workshop Localisation and Bifurcation Theory for Soils and Rocks*, Balkema, Rotterdam, 1994, pp. 113–126.
[7] D. Kolymbas, *Proc. 2nd Int. Conf. Constitutive Laws for Engineering Materials*, Elsevier, Amsterdam, 1987, p. 319.
[8] W. Wu and D. Kolymbas, *Mechan. Mater., 9* (1990) 245.
[9] W. Wu and Z. Sikora, *Int. J. Eng. Sci., 29* (1991) 195.
[10] E. Bauer and W. Wu, in D. Kolymbas (ed.), *Proc. Workshop Modern Approaches to Plasticity*, Elsevier, Amsterdam, 1993, pp. 247–258.
[11] W. Wu, E. Bauer, A. Niemunis and I. Herle, in D. Kolymbas (ed.), *Proc. Workshop Modern Approaches to Plasticity*, Elsevier, Amsterdam, 1993, pp. 365–383.
[12] W. Wu and A. Niemunis, Failure criterion, flow rule and dissipation function derived from hypoplasticity, *Int. J. Num. Anal. Methods Geomech.*, to be published.
[13] W. Wu and E. Bauer, in D. Kolymbas (ed.), *Proc. Workshop Modern Approaches to Plasticity*, Elsevier, Amsterdam, 1993, pp. 225–245.
[14] C. Truesdell and W. Noll, in S. Flügge (ed.), *Encyclopedia of Physics*, Vol. III, Springer, Berlin, 1965.
[15] C.C. Wang, *J. Rat. Mech. Anal., 36* (1970) 166.
[16] W. Wu, *Pub. Ser. Institute of Soil Mechanics and Rock Mechanics, No. 129*, Karlsruhe University, Germany, 1992.
[17] E. Bauer, *Publ. Ser. Institute of Soil Mechanics and Rock Mechanics, No. 130*, Karlsruhe University, Germany, 1992.
[18] H. Ziegler, *Quart. Appl. Math., 17* (1959) 55.
[19] A.N. Schofield and C.P. Wroth, *Critical State Soil Mechanics*, McGraw-Hill, London, 1968.
[20] J. Tejchmann and W. Wu, *Acta Mech., 99* (1993) 61.
[21] J. Harder, *Dissertation*, Technical University of Braunschweig, Germany, 1985.
[22] J. Schwedes and D. Schulze, *Powder Technol., 61* (1990) 59.